examined whether the mutation spectrum correlated with anatomical distribution and histological subtype. We initially grouped cerebral meningiomas into those originating along the skull base or those present in the cerebral hemispheres (Fig. 2E, fig. S7, and table S4). Interestingly, tumors with *NF2* mutations and/or chromosome 22 loss (*NF2/chr22loss*) were predominantly found in the hemispheres ($P = 9.22 \times 10^{-14}$; OR = 6.74) with nearly all posterior cerebral (parieto-occipital), cerebellar, or spinal meningiomas being *NF2/chr22loss* tumors (fig. S8). For the meningiomas originating from the skull base, we observed a difference between those originating from medial versus lateral regions. The vast majority of *non-NF2* meningiomas were medial ($P = 4.36 \times 10^{-8}$; medial versus lateral OR = 8.80), whereas the lateral and posterior skull base meningiomas had *NF2/chr22loss* ($P = 1.55 \times 10^{-12}$; OR = 23.11). Meningiomas with only the recurrent *SMO* L412F mutation ($n = 5$) all localized to the medial anterior skull base, near the midline. This is particularly interesting because mutations in Hedgehog signaling result in holoprosencephaly, the midline failure of embryonic forebrain to divide into two hemispheres (*12*).

Mutational profiles also were correlated with histological diagnoses. For example, all of the meningiomas with a "secretory" component ($n = 12$), which follow a more aggressive clinical course owing to increased brain swelling, carried both *TRAF7* and *KLF4* mutations ($P_{co} = 6.02 \times 10^{-12}$) (fig. S9).

Consistent with these clinical observations, unsupervised hierarchical clustering of meningiomas based on gene expression and chromatin immunoprecipitation for H3K27 acetylation followed by sequencing (H3K27ac ChIP-seq) analyses confirmed clustering into *NF2/chr22loss* versus *non-NF2* mutant subgroups (Fig. 2F and figs. S10 and S11) and revealed several molecules whose acetylation and expression was specific to a subtype (tables S5 and S6). For these differentially expressed genes, there was a strong correlation between expression and ChIP-seq data (fig. S12). Among the *non-NF2* meningiomas, *SMO* mutants were clearly defined by increased expression and activation of the Hedgehog pathway (fig. S13 and tables S7 and S8).

These results clearly identify meningioma subgroups, distinguishing them based on their mutually exclusive distribution of mutations, distinct potential for chromosomal instability and malignancy, anatomical location, histological appearance, gene expression, and H3K27ac profile. Our results show that the mutational profile of a meningioma can largely be predicted based on its anatomical position, which in turn may predict likely drug response (e.g., Hedgehog inhibitors for midline tumors). This may prove relevant for surgically unresectable, recurrent, or invasive meningiomas and could spare patients surgery or irradiation, an independent risk factor for progression of these generally benign tumors.

References and Notes

1. J. Wiemels, M. Wrensch, E. B. Claus, *J. Neurooncol.* **99**, 307 (2010).
2. M. J. Riemenschneider, A. Perry, G. Reifenberger, *Lancet Neurol.* **5**, 1045 (2006).
3. Materials and methods are available as supplementary materials on *Science* Online.
4. U. Schmitz *et al.*, *Br. J. Cancer* **84**, 199 (2001).
5. Q. Cui, *PLoS ONE* **5**, e13180 (2010).
6. L. G. Xu, L. Y. Li, H. B. Shu, *J. Biol. Chem.* **279**, 17278 (2004).
7. T. Bouwmeester *et al.*, *Nat. Cell Biol.* **6**, 97 (2004).
8. K. Takahashi *et al.*, *Cell* **131**, 861 (2007).
9. A. Schuetz *et al.*, *Cell. Mol. Life Sci.* **68**, 3121 (2011).
10. J. D. Carpten *et al.*, *Nature* **448**, 439 (2007).
11. J. Xie *et al.*, *Nature* **391**, 90 (1998).
12. E. Roessler *et al.*, *Nat. Genet.* **14**, 357 (1996).

Acknowledgments: We are grateful to the patients and their families who have contributed to this study. This study was supported by the Gregory M. Kiez and Mehmet Kutman Foundation. R.P.L. is an investigator of the Howard Hughes Institute. V.E.C. is supported by NIH T32GM07205. All somatic mutations identified through exome sequencing of meningiomas are reported in the supplementary materials and submitted to the Catalogue of Somatic Mutations in Cancer (COSMIC) database (http://cancer.sanger.ac.uk/cancergenome/projects/cosmic, submission ID COSP30702). Yale University has filed a provisional patent application based on the results of this study.

Supplementary Materials

www.sciencemag.org/cgi/content/full/science.1233009/DC1
Materials and Methods
Figs. S1 to S14
Tables S1 to S8
References (*13*–*27*)

24 May 2012; accepted 15 January 2013
Published online 24 January 2013;
10.1126/science.1233009

Unraveling the Mechanism of Protein Disaggregation Through a ClpB-DnaK Interaction

Rina Rosenzweig,[1,2,3]* Shoeib Moradi,[1] Arash Zarrine-Afsar,[2] John R. Glover,[1] Lewis E. Kay[1,2,3,4]*

HSP-100 protein machines, such as ClpB, play an essential role in reactivating protein aggregates that can otherwise be lethal to cells. Although the players involved are known, including the DnaK/DnaJ/GrpE chaperone system in bacteria, details of the molecular interactions are not well understood. Using methyl–transverse relaxation–optimized nuclear magnetic resonance spectroscopy, we present an atomic-resolution model for the ClpB-DnaK complex, which we verified by mutagenesis and functional assays. ClpB and GrpE compete for binding to the DnaK nucleotide binding domain, with GrpE binding inhibiting disaggregation. DnaK, in turn, plays a dual role in both disaggregation and subsequent refolding of polypeptide chains as they emerge from the aggregate. On the basis of a combined structural-biochemical analysis, we propose a model for the mechanism of protein aggregate reactivation by ClpB.

The 580-kD hexameric ClpB molecular chaperone is a bacterial adenosine 5′-triphosphate (ATP)–dependent protein-remodeling machine that rescues stress-damaged proteins trapped in an aggregated state and plays a key role in thermotolerance development and in cell recovery after acute stress (*1*–*3*). Aggregate reactivation requires the collaboration of a second ATP-dependent molecular chaperone system, Hsp70/DnaK (*1*, *4*–*7*). DnaK binding to client proteins is, in turn, regulated by co-chaperones DnaJ and GrpE through modulation of the DnaK ATPase cycle (*8*). A molecular picture of the ClpB-DnaK complex is critical to elucidate the mechanism of protein disaggregation, yet this system has proven recalcitrant to detailed structural studies.

Nuclear magnetic resonance (NMR) spectroscopy is especially suited to characterize protein complexes at atomic detail, even if the interactions are weak and transient. Methyl–transverse relaxation–optimized spectroscopy (TROSY)–based experiments (*9*) and labeling schemes, whereby Ile, Leu, and Val methyl groups are $^{13}CH_3$-labeled in an otherwise highly deuterated background (referred to as ILV-protein) (*10*), have enabled NMR studies of large molecular systems (*11*, *12*), such as those involved in disaggregation. Using these methods, we set out to elucidate the DnaK binding site on the ClpB chaperone.

Because of the large size of each monomer of ClpB (97 kD), NMR spectra of the ILV-labeled protein overlapped, precluding detailed analyses of the full-length molecule (fig. S1). We separately analyzed two monomeric fragments, including (i) $ClpB^{\Delta NBD2}$, comprising the N-terminal domain (NTD), nucleotide binding domain 1 (NBD1), and the coil-coil domain (CCD), and (ii) nucleotide

[1]Department of Biochemistry, University of Toronto, Toronto, Ontario M5S 1A8, Canada. [2]Department of Chemistry, University of Toronto, Toronto, Ontario M5S 3H6, Canada. [3]Department of Molecular Genetics, University of Toronto, Toronto, Ontario M5S 1A8, Canada. [4]Program in Molecular Structure and Function, Hospital for Sick Children, Toronto, Ontario M5G 1X8, Canada.

*To whom correspondence should be addressed. E-mail: rina.rosenzweig@utoronto.ca (R.R.); kay@pound.med.utoronto.ca (L.E.K.)

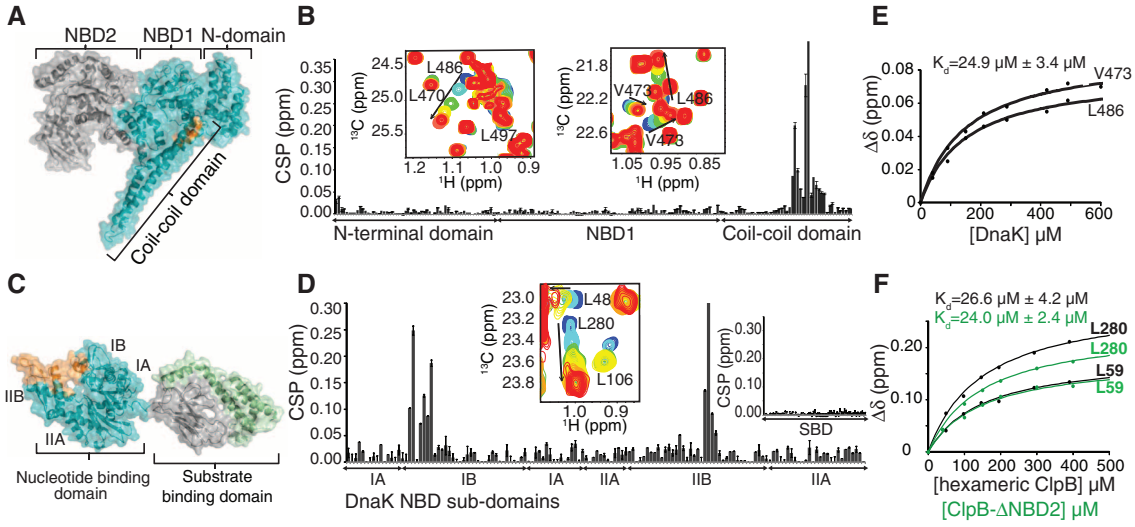

Fig. 1. Interaction between ClpB CCD and DnaK NBD as detected by NMR. (**A**) Monomer structure of ClpB [Protein Data Base (PDB): 1QVR] (*30*) highlighting each domain. Residues with CSPs upon addition of DnaK are colored orange. (**B**) (Top) Selected regions of ^{13}C-^{1}H HMQC data sets of ILV-ClpB$^{\Delta NBD2}$ in the absence (blue) or as a function of increasing concentrations (cyan to red) of 0.2 to 2.5 molar equivalents of unlabeled DnaK. Arrows indicate directions of peak movement. (Bottom) Magnitudes of CSPs for ILV- ClpB$^{\Delta NBD2}$ at the endpoint of titration with DnaK are shown as black bars for each residue. ClpB$^{\Delta NBD2}$ domains are indicated underneath. (**C**) Structural representation of DnaK chaperone, with residues showing significant CSPs highlighted in orange (see fig. S4C for details). The lid section of the SBD is shown in green. (**D**) (Top) Selected regions of HMQC spectra of ILV-DnaK in the absence (blue) and with increasing concentrations (cyan to red) of 0.2 to 2.0 molar equivalents of 580-kD hexameric, unlabeled ClpB. (Bottom) CSPs for ILV-DnaK as a function of residue number. DnaK^{NBD} subdomains are indicated underneath. (**E** and **F**) Titration curves, changes in chemical shifts Δδ versus concentration of titrant, and dissociation constant (K_d) values for the ClpB$^{\Delta NBD2}$-DnaK interaction, as described in the text.

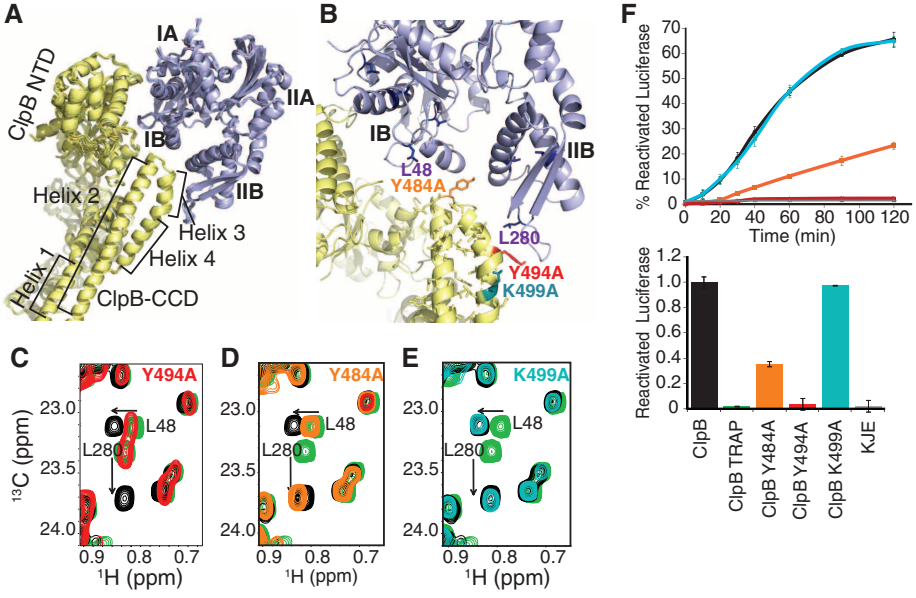

Fig. 2. Structural model for the ClpB-DnaK complex. (**A**) Ensemble of 10 lowest-energy HADDOCK structures for the ClpB$^{\Delta NBD2}$-DnaK complex. (**B**) Cartoon diagram of the lowest-energy structure from HADDOCK with detailed view on binding surface. (**C** to **E**) Key ClpB residues in contact with DnaK were mutated to Ala (Y494A-red, Y484A-orange, and K499A-blue) and complex formation was monitored by HMQC experiments that exploit a methyl-TROSY effect. CSPs for DnaK L48 and L280 from the unbound (green) to fully bound forms of DnaK (black) are shown in each spectrum as a reference. (**F**) (Top) Reactivation of luciferase aggregates monitored in the presence of indicated ClpB mutants and the DnaK/Dna]/GrpE (K/J/E) chaperone system. (Bottom) Reactivated luciferase after 120 min as a fraction of wt-ClpB reactivation. Standard errors of three independent assays are shown.

binding domain 2 (NBD2) (Fig. 1A). Of the two segments, only ILV-ClpB$^{\Delta NBD2}$ showed chemical-shift perturbations (CSPs) upon titration with unlabeled DnaK (Fig. 1B and fig. S1). Consistent with functional analyses of CCD mutants (*13*) and cross-linking results (*14*), the most prominent CSPs were mapped to specific residues in helices 2 and 3 of ClpB CCD (Fig. 1, A and B, and fig. S2), with several residues in the ClpB NTD showing very minor changes. To identify which DnaK residues participate in binding, additional titrations were performed with unlabeled hexameric ClpB added to ILV-DnaK, forming a 650-kD complex. The DnaK chaperone contains a pair of domains: an N-terminal nucleotide binding domain (NBD) and a C-terminal substrate binding domain (SBD) (Fig. 1C) that undergo substantial conformational changes during the ATPase-coupled substrate binding and release cycle of DnaK (*15*–*18*). CSPs of DnaK establish that NBD subdomains IB and IIB bind ClpB (Fig. 1D and fig. S3), whereas ClpB binding to the SBD was not detected (Fig. 1D and fig. S4). ^{15}N-^{1}H TROSY-HSQC (heteronuclear single-quantum coherence) experiments on smaller fragments such as a complex of ^{15}N-labeled DnaK^{NBD} and ClpB$^{NBD1\text{-}CCD}$ (fig. S4; 100-kD complex) confirmed and extended the ClpB interaction surface to the cleft between subdomains IB and IIB of DnaK and the extended loop of IIB. Similar binding affinities were obtained from the titration of ILV-ClpB$^{\Delta NBD2}$ with unlabeled-DnaK (Fig. 1E) and from titrations of ILV-DnaK with equivalent concentrations of either unlabeled hexameric ClpB or unlabeled monomeric ClpB$^{\Delta NBD2}$ (Fig. 1F and table S1), suggesting a 1:1 ClpB$_6$:DnaK stoichiometry (*19*).

Paramagnetic relaxation enhancement (PRE) experiments (*20*, *21*) were used to measure long-range distances between each of the components of the DnaK^{NBD}-ClpB$^{NBD1\text{-}CCD}$ (or DnaK^{NBD}-ClpB$^{\Delta NBD2}$) complex with nitroxide spin probes attached to one of residues 77, 222, 479, or 502 of ClpB (fig. S5). These distances were used in combination with CSPs as restraints in the flexible docking program HADDOCK (*22*, *23*) (table S2), with the resulting 95 docked structures (root mean

square deviation 0.41 Å) (table S3) revealing details of the DnaK NBD interaction with ClpB CCD (Fig. 2A). To cross-validate the ClpB-DnaK structural model, Y484 and Y494 in the ClpB CCD, potentially forming hydrogen bonds with R55 and K285 of DnaK subdomains IB and IIB, respectively (Fig. 2B), were mutated to Ala in $ClpB^{\Delta NBD2}$ and the interaction with DnaK monitored by NMR. Figure 2C illustrates a region of the ^{13}C-^{1}H HMQC (heteronuclear multiple-quantum coherence) map of ILV-DnaK unbound (green) or bound to wild-type (wt)–$ClpB^{\Delta NBD2}$ (black), overlaid on the spectrum obtained when $ClpB^{Y494A}$ is substituted for wt-$ClpB^{\Delta NBD2}$ (red). The superposition of "red" and "green" peaks establishes that complex formation does not occur with the Y494A mutant. Consistent with our model, CSPs for L280 and other methyl-containing probes of ILV-DnaK subdomain IIB titrated similarly for both wt-$ClpB^{\Delta NBD2}$ and $ClpB^{Y484A}$, indicating that the Y484A mutation does not disrupt contacts with subdomain IIB. By contrast, L48 (Fig. 2D) and other probes from ILV-DnaK subdomain IB showed no shifts upon addition of $ClpB^{Y484A}$, establishing that the Y484A mutation eliminates contacts with DnaK subdomain IB. Finally, $ClpB^{K499A}$, with position 499 located outside the DnaK binding surface, interacted with DnaK as the wild-type protein (Fig. 2E).

We tested the effect of these ClpB mutants on protein disaggregation by monitoring reactivation of aggregated firefly luciferase (Fig. 2F) and α-glucosidase (fig. S6). Both require tight collaboration between ClpB and DnaK chaperones, which we predicted depends on their physical interaction. $ClpB^{K499A}$ (hexamer), whose binding to DnaK is indistinguishable from that of wt-ClpB, was fully active in reactivation. However, as expected from the impaired binding observed by NMR, $ClpB^{Y484A}$ displayed a 65% reduction in reactivation compared to wt-ClpB. $ClpB^{Y494A}$, which did not bind DnaK in our NMR experiments, was correspondingly incapable of luciferase reactivation (Fig. 2F). None of the ClpB mutants showed defects in hexamer assembly or unfolding/translocation of nonaggregated unfolded protein (fig. S7).

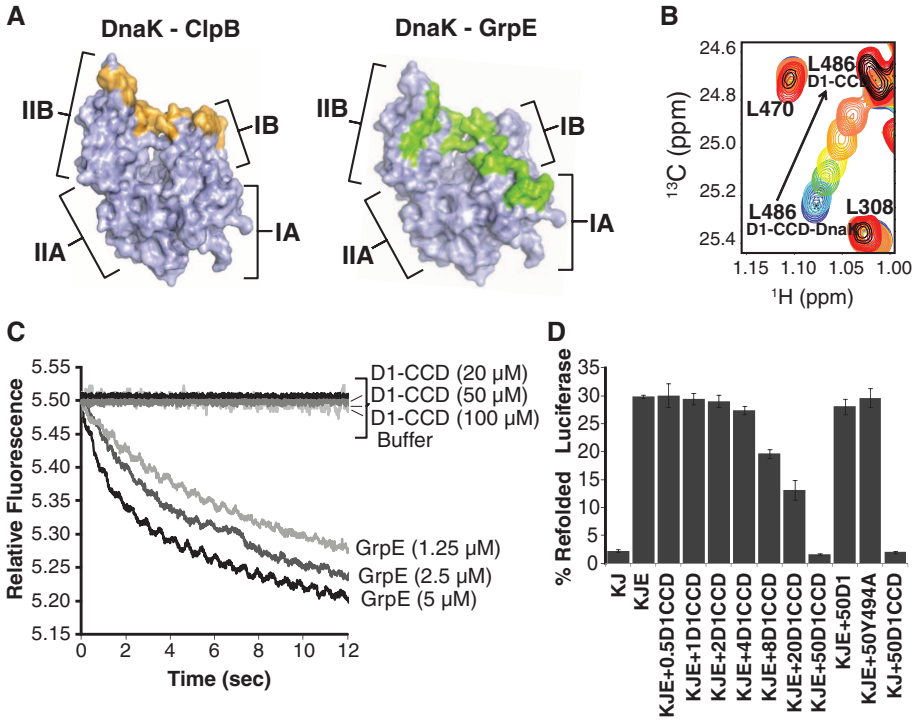

Fig. 3. The interaction of ClpB with DnaK competes with GrpE, yet does not induce nucleotide release. (**A**) DnaK residues that interact with ClpB (orange) and DnaK residues within 5 Å of GrpE [PDB: 1DKG (*24*)] in green. Subdomains are labeled for clarity. (**B**) Equimolar complex of ILV- $ClpB^{NBD1\text{-}CCD}$ and unlabeled DnaK (D1-CCD-DnaK, blue) was titrated with increasing concentrations of unlabeled GrpE, shifting peaks to their unbound position (D1-CCD, red). Peaks in black are from a spectrum of unbound NBD1-CCD. (**C**) Effect of GrpE or $ClpB^{NBD1\text{-}CCD}$ on nucleotide exchange rates of DnaK as monitored by stopped flow fluorimetry. (**D**) Percent luciferase refolding from soluble aggregates in the presence of the indicated chaperones. Addition of $ClpB^{NBD1\text{-}CCD}$ (D1CCD) inhibits refolding by the DnaK/DnaJ/GrpE (K/J/E) chaperone system, whereas addition of $ClpB^{NBD1}$ (D1) or CCD mutant Y494A (Y494A), which do not interact with DnaK, has no effect.

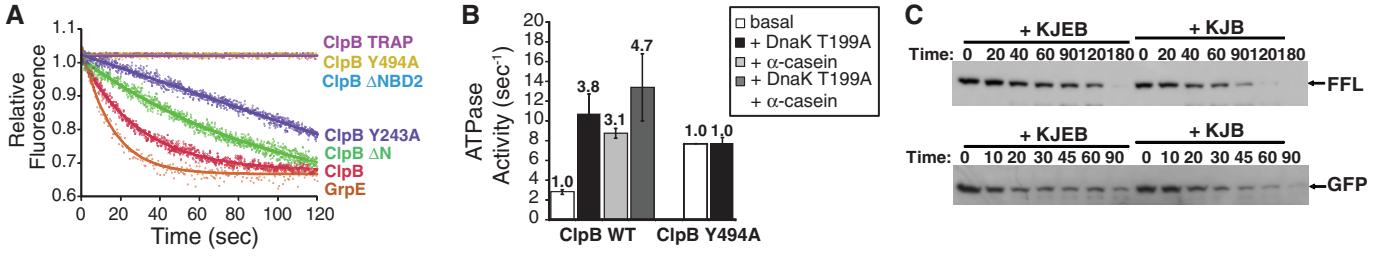

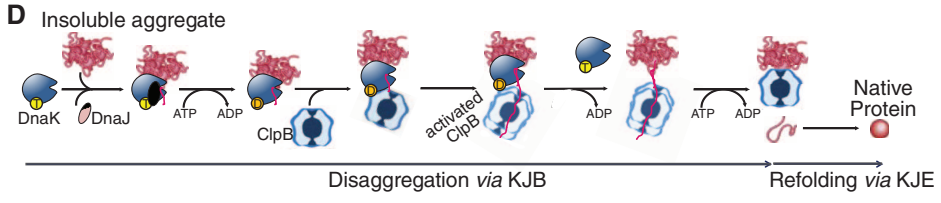

Fig. 4. The role of ClpB–DnaK collaboration in aggregate reactivation. (**A**) Dissociation of DnaK-RCMLa complex by the indicated proteins in the presence of ATP. The concentration of dimeric GrpE and hexameric ClpB were equivalent. (**B**) ATPase activity of ClpB is enhanced through interaction with DnaK or substrate α-casein. Rate of ClpB ATP hydrolysis was measured in the absence of other proteins (white bars), with $DnaK^{T199A}$ (black bars), with α-casein (light gray bars), or with both (dark gray bars). The higher basal ATPase activity of $ClpB^{Y494A}$ (*31*), which does not bind DnaK, was not stimulated in the presence of DnaK. (**C**) Coupled disaggregation/degradation reactions of aggregated firefly luciferase (FFL) and GFP (green fluorescent protein) by DnaK/DnaJ/GrpE/BAP/ClpP (KJEB) or DnaK/DnaJ/BAP/ClpP (KJB) monitored by Western blotting. Disaggregation rates are enhanced in the absence of GrpE. (**D**) Mechanistic model for collaboration between ClpB and DnaK systems in protein disaggregation.

The ClpB interaction with DnaK involves an extended loop in subdomain IIB (Figs. 2, A and B, and 3A) that also plays an important role in the binding of DnaK to the nucleotide exchange factor GrpE (Fig. 3A). Additionally, both ClpB and GrpE interact with the cleft between DnaK subdomains IB and IIB (Fig. 3A). Given these similarities, we determined whether GrpE and ClpB compete for DnaK binding. Addition of GrpE to an ILV-ClpB$^{NBD1\text{-}CCD}$–unlabeled DnaK complex caused shifting of cross peaks from residues in ClpB$^{NBD1\text{-}CCD}$ to their unbound position, confirming that GrpE and ClpB bind to the same surface of DnaK (Fig. 3B).

The GrpE interaction with DnaK leads to nucleotide dissociation and subsequent substrate release from DnaK (*24*). We tested whether ClpB-DnaK binding would also result in nucleotide release using the nucleotide MABA-ADP, which displays a decrease in fluorescence upon release from DnaK (*25*). Although increasing concentrations of GrpE enhanced adenosine 5′-diphosphate (ADP) release rates, ClpB$^{NBD1\text{-}CCD}$ could not stimulate ADP release from DnaK (Fig. 3C) or affect DnaJ-mediated DnaK ATP hydrolysis rates in the absence of GrpE (fig. S8).

Given that ClpB$^{NBD1\text{-}CCD}$ competes with GrpE for DnaK binding without promoting nucleotide exchange, we asked whether ClpB$^{NBD1\text{-}CCD}$ binding could hinder DnaK/DnaJ/GrpE–dependent refolding of heat-denatured substrates. Indeed, addition of ClpB$^{NBD1\text{-}CCD}$ reduced the yield of DnaK-reactivated luciferase or malate dehydrogenase MDH, with complete inhibition at a 50:1 ClpB$^{NBD1\text{-}CCD}$:GrpE ratio (Fig. 3D and fig. S8) that reflects the lower affinity of CCD relative to GrpE for DnaK.

Aggregate reactivation requires transfer of DnaK-bound client proteins to ClpB to facilitate protein disaggregation. Involvement of GrpE at this stage would disrupt the DnaK-ClpB interaction, substantially decreasing the efficiency of the disaggregation reaction. Thus, we explored the possibility of an alternative ClpB-dependent substrate release mechanism by monitoring the rates of RCMLa (reduced carboxymethylated lactalbumin) release from DnaK as a function of GrpE or ClpB variants (Fig. 4A). Surprisingly, ClpB could induce RCMLa release from DnaK nearly as efficiently as GrpE. When using ClpB^{Y243A}, a translocation-pore–deficient mutant, substrate release rates were reduced, indicating that the translocation activity of ClpB plays a role in this process. When an ATP-hydrolysis–deficient mutant, ClpB^{TRAP}, was used, no substrate release occurred, demonstrating a high dependence on ClpB ATPase activity and that binding to ClpB in and of itself is insufficient to promote substrate release from DnaK.

Given that ClpB ATPase activity is essential for substrate release from DnaK, we asked whether the ClpB-DnaK interaction has a functional role by tuning ClpB ATP turnover rates. ClpB ATP hydrolysis rates were measured in the presence or absence of either the substrate casein or a DnaK^{T199A} variant that cannot hydrolyze ATP. Interaction with either casein or DnaK separately increased ClpB ATP turnover rates between three- and fourfold, with a fivefold increase when both DnaK and α-casein were added (Fig. 4B and fig. S7). Furthermore, ClpB CCD can convert ClpB from a repressed state to an activated state in a DnaK-dependent manner (*14*). Thus, direct interaction of ClpB CCD with DnaK increases ClpB ATPase activity, which in turn enhances ClpB substrate threading power.

The DnaK chaperone system is active both upstream of ClpB, where it aids in extracting polypeptides from aggregates (*26*), and downstream, where DnaK/DnaJ/GrpE refold polypeptide chains that emerge from the ClpB lumen (*5*). We tested whether GrpE is required in the initial steps of the disaggregation reaction by performing disaggregation assays with and without this co-chaperone in a manner that eliminates the need for downstream GrpE-dependent refolding by using (i) a modified version of ClpB, termed BAP (*3*), that binds to the ClpP protease and transfers substrates emerging from the BAP central pore directly to ClpP for degradation or (ii) wt-ClpB/DnaK/DnaJ in combination with refolding chaperones GroEL/ES. In both cases, the presence of GrpE was detrimental to disaggregation (Fig. 4C and fig. S9). This reflects the competition between GrpE and ClpB for DnaK binding that leads to premature release of ClpB from the aggregate. Thus, the biological function of GrpE is solely downstream of the DnaK-ClpB disaggregation reaction. Indeed, GrpE is reversibly inactivated during heat shock (*27*, *28*), which explains the ability of ClpB and DnaK to solubilize cellular aggregates without interference from GrpE under stress conditions.

We propose a mechanism by which the ClpB and DnaK chaperone systems reactivate insoluble protein aggregates (Fig. 4D). DnaK/DnaJ act during the early stages of aggregate reactivation, exposing peptide segments that then serve as the initiating points for disaggregation (*29*). These exposed segments of the aggregated protein are brought to the substrate-processing central pore of ClpB through direct interaction between the DnaK NBD and ClpB CCD. Association of either DnaK or substrate with ClpB leads to its activation, with nucleotide turnover rates greatly amplified in the presence of both. Activated ClpB then pulls on exposed regions of peptide chains in the aggregate, progressively unfolding and threading them through its axial channel (*3*). Once unfolded substrates emerge from the ClpB central pore, they either refold spontaneously or are recovered by the DnaK/DnaJ/GrpE system.

References and Notes

1. D. A. Parsell, A. S. Kowal, M. A. Singer, S. Lindquist, *Nature* **372**, 475 (1994).
2. Y. Sanchez, S. L. Lindquist, *Science* **248**, 1112 (1990).
3. J. Weibezahn *et al.*, *Cell* **119**, 653 (2004).
4. J. R. Glover, S. Lindquist, *Cell* **94**, 73 (1998).
5. P. Goloubinoff, A. Mogk, A. P. Zvi, T. Tomoyasu, B. Bukau, *Proc. Natl. Acad. Sci. U.S.A.* **96**, 13732 (1999).
6. A. Mogk *et al.*, *EMBO J.* **18**, 6934 (1999).
7. K. Motohashi, Y. Watanabe, M. Yohda, M. Yoshida, *Proc. Natl. Acad. Sci. U.S.A.* **96**, 7184 (1999).
8. M. P. Mayer, B. Bukau, *Cell. Mol. Life Sci.* **62**, 670 (2005).
9. V. Tugarinov, P. M. Hwang, J. E. Ollerenshaw, L. E. Kay, *J. Am. Chem. Soc.* **125**, 10420 (2003).
10. V. Tugarinov, L. E. Kay, *J. Biomol. NMR* **28**, 165 (2004).
11. R. Sprangers, L. E. Kay, *Nature* **445**, 618 (2007).
12. I. Gelis *et al.*, *Cell* **131**, 756 (2007).
13. M. Miot *et al.*, *Proc. Natl. Acad. Sci. U.S.A.* **108**, 6915 (2011).
14. F. Seyffer *et al.*, *Nat. Struct. Mol. Biol.* **19**, 1347 (2012).
15. K. M. Flaherty, C. DeLuca-Flaherty, D. B. McKay, *Nature* **346**, 623 (1990).
16. M. Sriram, J. Osipiuk, B. Freeman, R. Morimoto, A. Joachimiak, *Structure* **5**, 403 (1997).
17. A. Zhuravleva, E. M. Clerico, L. M. Gierasch, *Cell* **151**, 1296 (2012).
18. R. Kityk, J. Kopp, I. Sinning, M. P. Mayer, *Mol. Cell* **48**, 863 (2012).
19. See supplementary materials on *Science* Online.
20. J. L. Battiste, G. Wagner, *Biochemistry* **39**, 5355 (2000).
21. T. L. Religa, R. Sprangers, L. E. Kay, *Science* **328**, 98 (2010).
22. C. Dominguez, R. Boelens, A. M. Bonvin, *J. Am. Chem. Soc.* **125**, 1731 (2003).
23. S. J. de Vries *et al.*, *Proteins* **69**, 726 (2007).
24. C. J. Harrison, M. Hayer-Hartl, M. Di Liberto, F. Hartl, J. Kuriyan, *Science* **276**, 431 (1997).
25. Y. Groemping *et al.*, *J. Mol. Biol.* **305**, 1173 (2001).
26. C. Schlieker, I. Tews, B. Bukau, A. Mogk, *FEBS Lett.* **578**, 351 (2004).
27. J. P. Grimshaw, I. Jelesarov, H. J. Schönfeld, P. Christen, *J. Biol. Chem.* **276**, 6098 (2001).
28. Y. Groemping, J. Reinstein, *J. Mol. Biol.* **314**, 167 (2001).
29. T. Haslberger *et al.*, *Nat. Struct. Mol. Biol.* **15**, 641 (2008).
30. S. Lee *et al.*, *Cell* **115**, 229 (2003).
31. T. Haslberger *et al.*, *Mol. Cell* **25**, 247 (2007).

Acknowledgments: We thank J. Forman-Kay for providing laboratory space and for valuable discussions, R. Muhandiram for NMR support, and M. Latham for helpful discussions. wt-ClpB and GroEL/ES constructs were generously provided by F. Tsai (Baylor College of Medicine, Texas) and A. Horwich (Yale School of Medicine, Connecticut). R.R. acknowledges the European Molecular Biology Organization (ALTF-570-2010) and the Government of Canada (Banting) for postdoctoral fellowships. L.E.K. holds a Canada Research Chair in Biochemistry. This work was supported by a grant from the Canadian Institutes of Health Research. Coordinates for the ClpB-DnaK complex are available as supplementary material.

Supplementary Materials

www.sciencemag.org/cgi/content/full/science.1233066/DC1
Materials and Methods
Figs. S1 to S9
Tables S1 to S3
References (*32*–*66*)
Coordinates for ClpB-DNA complex

21 November 2012; accepted 23 January 2013
Published online 7 February 2013;
10.1126/science.1233066

Science

Unraveling the Mechanism of Protein Disaggregation Through a ClpB-DnaK Interaction

Rina Rosenzweig, Shoeib Moradi, Arash Zarrine-Afsar, John R. Glover, and Lewis E. Kay

Science, 339 (6123), • DOI: 10.1126/science.1233066

Dissecting Disaggregation

The excessive accumulation of misfolded protein aggregates can overwhelm the cell's "quality control" machinery, leading to cell death. The yeast Hsp104 protein and its bacterial homolog ClpB are molecular chaperones that can "rescue" aggregated proteins by coupling the force generated from adenosine triphosphate hydrolysis to the progressive unfolding and threading of extended polypeptide segments through axial channels in these large molecular machines. Unfolded polypeptides emerging from the channel are refolded with the aid of a second chaperone system, DnaK/DnaJ/GrpE. DnaK also plays an important role in bringing regions of polypeptides within aggregates to ClpB to begin the solubilization process. Rosenzweig *et al.* (p. 1080, published online 7 February; see the Perspective by Saibil) describe a nuclear magnetic resonance–derived structure of the ClpB-DnaK complex, and verified it through mutagenesis and functional assays. The work clarifies the roles of each of the molecular players in the disaggregation reaction and provides a structural basis for the DnaK-ClpB interaction.

View the article online
https://www.science.org/doi/10.1126/science.1233066
Permissions
https://www.science.org/help/reprints-and-permissions

Use of this article is subject to the Terms of service

Science (ISSN 1095-9203) is published by the American Association for the Advancement of Science. 1200 New York Avenue NW, Washington, DC 20005. The title *Science* is a registered trademark of AAAS.
Copyright © 2013, American Association for the Advancement of Science